

only listen to the nature of the sounds they produce, but also look at the reactions their sounds provoke.

Financial assistance was provided by the NSF and the National Institute of Neurological and Communicative Disorders and Strokes.

Received 11 March; accepted 31 May 1988.

1. Petrinovich, L. in *Social Learning: Psychological and Biological Perspectives* (eds Zentall, T. & Galef, B. G.) 255-278 (Lawrence Erlbaum, New York, 1988).
2. King, A. P. & West, M. J. *Nature* **305**, 704-706 (1983).
3. West, M. J. & King, A. P. *Ethology* **70**, 225-235 (1985).
4. King, A. P. & West, M. J. *Anim. Behav.* (in the press).
5. Kroodsma, D. E. in *Acoustic Communication in Birds* Vol. 2 (eds Kroodsma, D. E. & Miller, E. H.) 1-28 (Academic Press, New York, 1982).
6. West, M. J. & King, A. P. *J. comp. Psychol.* **100**, 296-303 (1986).
7. McGregor, P. K. & Krebs, J. P. *Behaviour* **79**, 127-147 (1982).

## Acetylcholine inhibits identified interneurons in the cat lateral geniculate nucleus

David A. McCormick & Hans-Christian Pape

Section of Neuroanatomy, Yale University School of Medicine,  
333 Cedar Street, New Haven, Connecticut 06510, USA

The transmission of visual information from retina to cortex through the dorsal lateral geniculate nucleus (LGNd) is controlled by non-retinal inputs<sup>1,2</sup>. Enhanced visually evoked responses in cat LGNd relay cells during periods of increased alertness<sup>3</sup> have been attributed in large part to increased rate of acetylcholine (ACh) release by fibres ascending from the brainstem reticular formation<sup>4-7</sup>. ACh can modulate geniculate visual responses *in vivo*<sup>5-8</sup>, but comparatively little is known about the underlying ionic mechanisms of these cholinergic actions. Although direct excitation of LGNd relay neurons has been shown *in vitro*<sup>9</sup>, the situation is complicated because cholinergic axons form numerous and complex synapses not only with relay cells, but also with inhibitory interneurons<sup>10</sup>, and electrical activation of the brainstem cholinergic neurons reduces inhibitory postsynaptic potentials in the LGNd<sup>11-13</sup>. We report here that morphologically characterized interneurons in the cat LGNd possess distinctive electrophysiological properties in comparison with those of relay cells and are inhibited by ACh through a muscarinic receptor-mediated increase in potassium conductance. Together the direct excitation of relay cells and inhibition of intrageniculate interneurons allow the ascending cholinergic system to exert a powerful facilitatory influence over the transfer of visual information to the cerebral cortex.

Intracellular recordings from cells in lamina A or A<sub>1</sub> of the cat LGNd revealed two distinct classes of neurons, which we tentatively term principal (P) and I neurons. P neurons display electrophysiological properties similar to those reported previously for thalamocortical relay cells<sup>14-16</sup>, including the presence of a low threshold Ca<sup>2+</sup> spike which underlies burst discharges (Fig. 1e, arrow head), anomalous rectification in both the hyperpolarizing (Fig. 1e) and depolarizing ranges (data not shown), a delayed onset to firing during depolarization (Fig. 1c, arrow head), and a general lack of pronounced spike frequency accommodation (Fig. 1c).

In contrast, we found that I neurons either lack completely a typical low threshold Ca<sup>2+</sup> spike (Fig. 1f; *n* = 4) or display only a small rebound exultation after a large hyperpolarization (data not shown; *n* = 4). Furthermore, I neurons possess action potentials which are on the average 28% shorter in duration than those of P cells (compare Fig. 1a and b), lack a delayed onset to firing (Fig. 1d), display more linear membrane potential versus injected current (*V*-*I*) relationships, and have a higher input resistance (I neurons: 89 ± 24 MΩ (mean ± s.d.), *n* = 9;

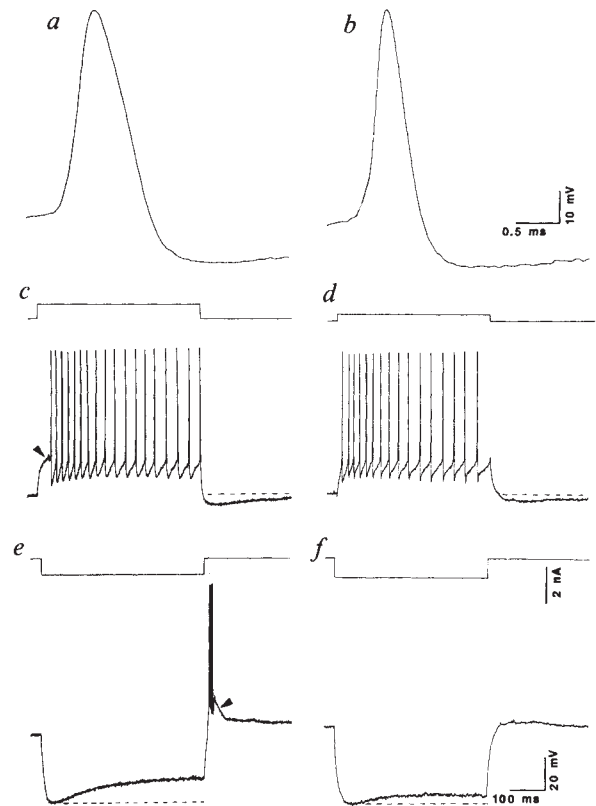


**Fig. 1** Electrophysiological properties of LGNd P and I neurons. *a* and *b*, Single action potential of a typical P cell (*a*, 0.52 ms) is substantially broader at half peak amplitude than that of a typical I neuron (*b*, 0.31 ms) (average action potential duration ± s.d. for the two groups: P cells, 0.50 ± 0.20 ms, *n* = 20; I neurons, 0.36 ± 0.13 ms, *n* = 13; *t* = 2.27, *P* < 0.05). *c* and *d*, Responses to a depolarizing current pulse of a P cell (the same I neuron; resting membrane potential (*V*<sub>m</sub>) = -64 mV; arrow head indicates delayed onset of firing) and an I neuron (*d*; resting *V*<sub>m</sub> = -76 mV). *e* and *f*, Injection of hyperpolarizing current pulses into a typical P cell (*e*) and an I neuron (*f*). Note the lack of a rebound low threshold Ca<sup>2+</sup> spike in the I neuron (*f*) versus the P cell (*e*, arrow head; burst contains four action potentials) despite the large hyperpolarization from -76 to -135 mV. All data in *a*, *c* and *e* are from the same P cell and those from *b*, *d* and *f* are from the same I neuron. Calibration bars in *f* for *c*-*f*, calibration bars in *b* for *a* and *b*. Top trace in *c*-*f* is injected current, whereas the bottom trace is the resulting deviation in *V*<sub>m</sub>.

**Methods.** Eleven 3-month to 3-year old cats were deeply anaesthetized with ketamine (20 mg per kg, intramuscularly) and sodium pentobarbital (15 mg per kg, intravenously) and underwent a wide craniotomy. The animals were killed by decapitation and both hemispheres were rapidly removed and dissected to isolate the lateral geniculate nucleus which was then sectioned coronally on a vibratome as 400 μm slices. Slices were maintained in an interface chamber at 35 ± 1 °C and perfused with a solution containing (in mM) NaCl, 126; KCl, 2.5; MgSO<sub>4</sub>, 2; NaHCO<sub>3</sub>, 26; NaH<sub>2</sub>PO<sub>4</sub>, 1.25; CaCl<sub>2</sub>, 2; glucose, 10; saturated with 95% O<sub>2</sub>, 5% CO<sub>2</sub> to a final pH of 7.4. Epi-illumination of the coronal slices readily revealed the main laminae of the LGNd as well as the optic tract and optic radiation. Neurons were recorded only in the middle portions of laminae A and A<sub>1</sub> to avoid recording from perigeniculate or interlaminar cells. Microelectrodes were filled with 4 M KAc for normal recordings and 0.2 M LiCl saturated with lucifer yellow CH (LY) for intracellular labelling experiments. Only neurons having stable membrane potentials below -55 mV and overshooting action potentials were included in the electrophysiological analysis. Action potential durations were measured at half-peak amplitude. Acetylcholine (ACh, 10 mM) or acetyl-β-methylcholine (MCh, 10 mM) were applied from a broken micropipette (1-2-μm tip diameter) by pressure pulses in volumes of approximately 10 pl within 50-75 μm of the recorded cell. LGNd slices containing LY-labelled neurons were resectioned at 50-75 μm, mounted and cleared on microscopic slides, and photographed.

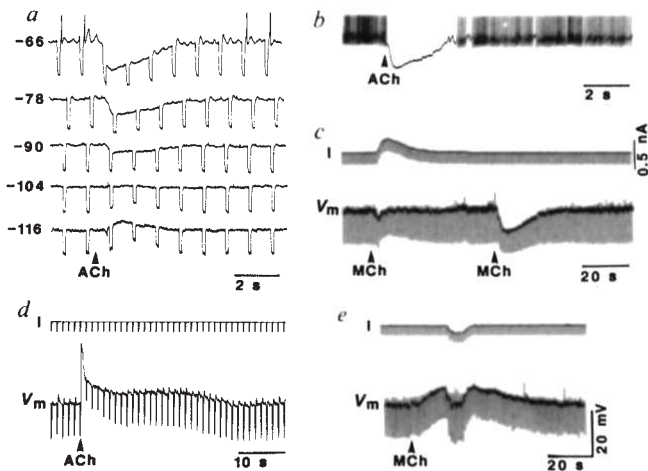


**Fig. 2** Actions of acetylcholine on P and I neurons in the LGNd. *a*, Application of ACh to the I neuron illustrated in Fig. 1 results in membrane hyperpolarization which reverses to a depolarization at about  $-104$  mV. *b*, Application of ACh to the neuron of *a* during steady depolarization to evoke spiking causes inhibition with no evidence of fast or slow excitation. *c*, MCh hyperpolarizes the I neuron (second application), and manual voltage clamp reveals the response to be associated with a substantial increase in  $G_i$  (first application). *d*, Application of ACh to a typical P cell results in a rapid depolarization followed by a slow depolarization. *e*, MCh causes the slow depolarization only (same neuron as in *d*). Compensation for the depolarization with inward current injection reveals the response to be associated with a decrease in  $G_i$ .

P cells,  $51 \pm 20$  M $\Omega$ ;  $n = 20$ ;  $t = 4.5$ ,  $P < 0.001$ ).

Application of acetylcholine to P cells at resting membrane potential causes a rapid depolarization, followed by a slower depolarization of smaller amplitude (Fig. 2*d*), as previously reported<sup>9</sup>. The fast depolarization, associated with a substantial increase in apparent input conductance ( $G_i$ ), often elicits spike discharges, whereas the slow depolarization, associated with a decrease in  $G_i$ , reaches threshold for neuronal firing only from more depolarized membrane potentials. The muscarinic agonist, acetyl- $\beta$ -methylcholine (MCh) evokes the slow depolarization and decrease in  $G_i$  only (Fig. 2*e*), which in some neurons is preceded by a small hyperpolarization<sup>9</sup>.

In contrast to cholinergic actions on P cells, application of ACh to electrophysiologically identified I neurons results in only a hyperpolarization and inhibition of spike discharge with no indication of fast or slow depolarizing effects ( $n = 9/11$  (two cells showed no response); Figs 2*a*, *b* and 3*d*). Like ACh, the muscarinic agonist, MCh elicits a membrane hyperpolarization associated with an increase in  $G_i$  (Fig. 3*d*). Unlike reticular thalamic neurons<sup>17</sup>, the muscarinic hyperpolarization does not promote the occurrence of burst discharges in I neurons, due to an absence of a typical low threshold  $Ca^{2+}$  spike.

Possible ionic conductances underlying the ACh-induced hyperpolarization were investigated by applying ACh while the I neurons were positioned at various membrane potentials (Figs 2*a* and 3*d*). The ACh response reverses at an average membrane potential of  $-102.4 \pm 4.8$  mV ( $n = 3$ ), which is similar to the presumed potassium equilibrium potential of thalamic neurons<sup>17</sup>. These results indicate that ACh inhibits I neurons by increasing a membrane potassium conductance mediated through muscarinic receptors, similar to that reported previously in other mammalian central nervous system neurons<sup>17,18</sup>.

To test the hypothesis that the two electrophysiologically and pharmacologically defined subclasses of LGNd neurons may possess distinct morphological features, we intracellularly labelled recorded neurons with the fluorescent dye lucifer yellow CH. All of the cells demonstrating the electrophysiological

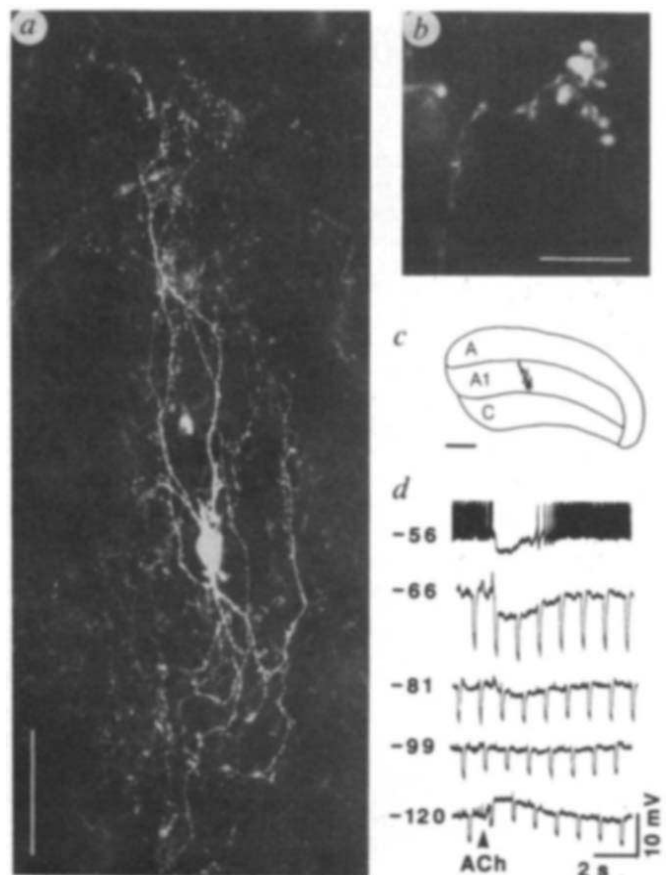


**Fig. 3** Morphological characteristics of electrophysiologically and pharmacologically defined LGNd I neurons. *a*, Photomicrograph of a  $75\text{-}\mu\text{m}$  section containing a LY-filled I neuron exhibiting typical type-3 morphological characteristics. Scale bar equals  $50\ \mu\text{m}$ . *b*, Typical terminal ending of a dendritic process of the neuron in *a*. Scale bar equals  $10\ \mu\text{m}$ . *c*, Position of the same neuron in the LGNd slice. Scale bar equals  $300\ \mu\text{m}$ . *d*, Hyperpolarizing response of the neuron in *a* to application of ACh. Reversal potential is  $-99$  mV.

properties mentioned above for P cells were found to possess somatic and dendritic morphologies which are typical for either type-1 ( $n = 14$ ) or type-2 ( $n = 9$ ) relay cells as defined by Guilley<sup>19</sup>. Axons of P cells were often observed to enter into the optic radiation (data not shown). In contrast, injection of lucifer yellow into electrophysiologically identified I neurons ( $n = 12$ ) revealed in every case cells with somatic and dendritic morphologies typical for Guilley type-3 cells<sup>19,20</sup> which have recently been shown to be interneurons that contain  $\gamma$ -aminobutyric acid (GABA)<sup>21</sup>. Their morphological features included small cell bodies (type-3 cells:  $17.6 \pm 3.6$  by  $11.0 \pm 3.1\ \mu\text{m}$  diameter; compare with type-1 cells:  $24.5 \pm 3.1$  by  $17.3 \pm 4.1\ \mu\text{m}$ ; type-2 cells:  $19.7 \pm 3.5$  by  $12.4 \pm 2.9\ \mu\text{m}$ ) and thin, sinuous, 'axon-like' dendrites which possess numerous filiform appendages ending in characteristic 'synaptic knobs' (Fig. 3*a*, *b*). None of the identified type-3 neurons possess a detectable axon which leaves the local neuronal environment. Figure 3 shows the detailed properties of a morphological type-3 neuron. Its numerous thin dendrites arborize extensively in a bitufted manner transverse to the long axis of the LGNd (Fig. 3*a*, *c*) and possess filiform appendages and putative synaptic terminals characteristic of intrageniculate interneurons (Fig. 3*b*). Application of ACh to morphologically identified type-3 cells ( $n = 5$ ) results in the typical hyperpolarization and associated increase in membrane conductance (Fig. 3*d*), confirming our results obtained with electrophysiologically identified I neurons.

Stimulation, microiontophoretic and neuroanatomical tracing experiments have indicated that the brainstem cholinergic system is critically involved in the ascending control of geniculate neuronal responsiveness<sup>1-13,22-26</sup>. In the LGNd, acetylcholine is thought to increase relay cell excitability during periods of alertness by direct excitation and by interaction with inhibitory mechanisms<sup>3,5-9,22</sup>. Our results demonstrate two distinct mechanisms by which the ascending cholinergic projection system facilitates the relay of visual information through the LGNd. The direct depolarization of relay neurons by ACh is expected to inhibit ongoing burst discharges and to bring the cell's membrane potential closer to the optimal level for the accurate transfer of incoming excitatory inputs. The inhibition of local GABAergic inhibitory interneurons by ACh will further facilitate the responsiveness of the relay neurons to excitatory inputs. Also, the inhibitory feedback loop to the LGNd via the perigeniculate nucleus, which is believed to be critical in the generation of rhythmic burst discharges of slow wave sleep<sup>24</sup>, is inhibited by ACh<sup>5-7,17,22,23</sup>. The presence of a widespread cholinergic innervation of the thalamus<sup>25</sup> indicates that these results may generalize to other sensory-motor systems and as such may form a basis for the ascending control of arousal.

This work was supported by the Jacob Javits Center for

Excellence in Neuroscience, and a fellowship of the Deutsche Forschungsgemeinschaft to H.-C.P.

Received 9 May; accepted 23 May 1988.

1. Singer, W. *Physiol. Rev.* **57**, 386-420 (1977).
2. Sherman, S. M. & Koch, C. *Expl. Brain Res.* **63**, 1-20 (1986).
3. Livingstone, M. S. & Hubel, D. H. *Nature* **291**, 554-561 (1981).
4. Phillips, J. W., Tebécis, A. K. & York, D. H. *J. Physiol.* **192**, 695-713 (1967).
5. Sillito, A. M., Kemp, J. A. & Berardi, N. *Brain Res.* **280**, 299-307 (1983).
6. Eysel, U. T., Pape, H.-C. & Van Schayck, R. *J. Physiol.* **370**, 233-254 (1986).
7. Francesconi, W., Müller, C. M. & Singer, W. *J. Neurophysiol.* (in the press).
8. Eysel, U. T., Pape, H.-C. & Van Schayck, R. *J. Physiol.* **388**, 199-212 (1987).
9. McCormick, D. A. & Prince, D. A. *J. Physiol.* **392**, 147-165 (1987).
10. De Lima, A. D., Montero, V. M. & Singer, W. *Expl. Brain Res.* **59**, 206-212 (1985).
11. Singer, W. & Dräger, U. *Brain Res.* **41**, 214-220 (1972).
12. Singer, W. *Brain Res.* **61**, 35-54 (1973).
13. Ahlsén, G., Lindström, S. & Lo, F.-S. *J. Physiol.* **347**, 593-609 (1984).
14. Jahnsen, H. & Llinás, R. *J. Physiol.* **349**, 205-226 (1984).
15. Jahnsen, H. & Llinás, R. *J. Physiol.* **349**, 227-247 (1984).
16. Crunelli, V., Haby, M., Jassik-Gerschenfeld, D., Leresche, N. & Pirchio, M. *J. Physiol.* **399**, 153-176 (1988).
17. McCormick, D. A. & Prince, D. A. *Nature* **319**, 402-405 (1986).
18. Egan, T. M. & North, R. A. *Nature* **319**, 405-407 (1986).
19. Guillery, R. W. *J. comp. Neurol.* **128**, 21-50 (1966).
20. Hamos, J. E., Van Horn, S. C., Raczkowski, D., Uhlrich, D. J. & Sherman, S. M. *Nature* **317**, 618-621 (1985).
21. Montero, V. M. *J. comp. Neurol.* **254**, 228-245 (1986).
22. Pape, H.-C. & Eysel, U. T. *Brain Res.* **440**, 79-86 (1988).
23. Godfraind, J. M. *Br. J. Pharmac.* **63**, 295-302 (1978).
24. Steriade, M. & Deschênes, M. *Brain Res. Rev.* **8**, 1-63 (1984).
25. Rye, D. B., Saper, C. B., Lee, H. J. & Wainer, B. H. *J. comp. Neurol.* **259**, 483-528 (1987).
26. De Lima, A. D. & Singer, W. *J. comp. Neurol.* **259**, 92-121 (1987).

## Mapping of mutation causing Friedreich's ataxia to human chromosome 9

Susan Chamberlain, Jacqui Shaw, Alison Rowland, Julie Wallis, Sally South, Yusuke Nakamura\*, Alexander von Gabain†, Martin Farrall & Robert Williamson

Department of Biochemistry and Molecular Genetics, Saint Mary's Hospital Medical School, University of London, London W2 1PG, UK

\* Howard Hughes Medical Institute, University of Utah School of Medicine, Salt Lake City, Utah 84123, USA

† Department of Bacteriology, Karolinska Institutet, Box 60400, 104 01 Stockholm, Sweden

Friedreich's ataxia is an autosomal recessive disease with progressive degeneration of the central and peripheral nervous system<sup>1,2</sup>. The biochemical abnormality underlying the disorder has not been identified. Prompted by the success in localizing the mutations causing Duchenne muscular dystrophy<sup>3,4</sup>, Huntington's disease<sup>5</sup> and cystic fibrosis<sup>6-8</sup>, we have undertaken molecular genetic linkage studies to determine the chromosomal site of the Friedreich's ataxia mutation as an initial step towards the isolation and characterization of the defective gene. We report the assignment of the gene mutation for this disorder to chromosome 9p22-CEN by genetic linkage to an anonymous DNA marker MCT112 and the interferon- $\beta$  gene probe. In contrast to the clinical variation seen for the disorder, no evidence of genetic heterogeneity is observed.

The incidence of Friedreich's ataxia is approximately one in fifty thousand. Collaboration with colleagues in Europe and the United States was required to establish a collection of 22 families with three or more affected siblings, to carry out an effective linkage study. Fourteen of these pedigrees have previously been described<sup>9</sup>. Compliance with the diagnostic criteria of Geoffroy *et al.*<sup>1</sup> was observed to minimize the risk of clinical heterogeneity within the sample population.

The possibility that Friedreich's ataxia may be caused by mutations of several different genes, with one predominant mutation, has been discussed by Harding<sup>10</sup>. For the purposes

of this study we have assumed that the disease is a single-gene disorder, where variation in symptoms (such as age of onset and severity) probably result from different mutations at the same locus.

We have analysed 117 informative cloned DNA markers for linkage to Friedreich's ataxia<sup>9,11</sup>, as well as 36 polymorphic blood group and protein markers, the latter in collaboration with colleagues in the United States, Denmark and Canada<sup>12</sup>. These studies have served to exclude the disease gene from close proximity to these markers if a lod score ( $\log_{10}$  odds ratio) of  $-2$  or less was generated<sup>13</sup>, usually at a recombination fraction of at least  $\theta = 0.10$ .

Analysis of the combined data using the EXCLUDE program<sup>14</sup>, which calculates the likelihood distribution around a series of previously mapped loci, generated an exclusion map for more than 80% of the genome. Statistically, three chromosomal regions were emphasized as the most probable sites for the Friedreich's ataxia mutation. Intensive investigation of these regions led to the demonstration of linkage between the mutation causing the disease and two markers on chromosome 9, the interferon- $\beta$  gene (INFB) and the anonymous probe MCT112,

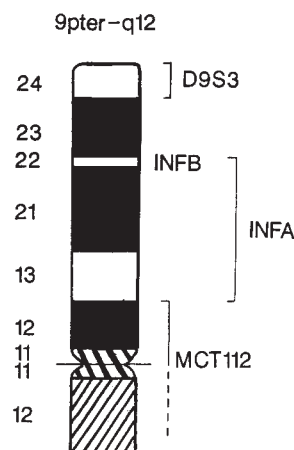


Fig. 1 Chromosome 9pter-q12. Physical assignment of the interferon- $\beta$  gene and the locus defined by the DNA marker MCT112 by genetic linkage analysis.